Three-Dimensional Model of Fracture Propagation from the Cavity Caused by Quasi-Static Load or Viscous Fluid Pumping

Yuriy Shokin, Sergey Cherny, Denis Esipov, Vasily Lapin, Alexey Lyutov, and Dmitriy Kuranakov(✉)

Institute of Computational Technologies of the SB RAS,
Acad. Lavrentjev, 6, 630090 Novosibirsk, Russia
{esipov,lapin,kuranakov}@ict.sbras.ru
http://www.ict.nsc.ru/ru/

Abstract. Fracture propagation caused by fluid pumping is in the focus of the report. The most popular approaches and problem statements used for the propagation simulation are described.

Methods of simulation of the main processes that take place during the fracture propagation are outlined. There processes are the follows: rock deformation and rock breaking, fluid flow inside the fracture and its filtration in the rock.

New method of fracture propagation simulation is proposed. The method unites three sub-models that describe three (except the fluid filtration) processes that affect the fracture propagation. Important advance of the methodic is its ability to replace any sub-model without numerical algorithm modification. So the appropriate sub-model can be chosen for each process depending on the problem features.

Thus quasi static and unsteady statement may be used for simulation of fracture propagation caused by viscous and inviscid fluid pumping. Rock deformation is described in scope of linear elasticity equation of homogeneous uniform material. Classical (similar to one used in [1]) and dual boundary element methods are used for this equations solution. Rock breaking caused by the fracture propagation is described by Irwin's criterion coupled with maximal circumferential stress criterion for calculation of propagation direction. Various approaches are used to obtain stress intensity factors that are necessary for both criteria.

Proposed methodic has been applied for fracture propagation simulation. The sensitivity of fracture propagation process to variation of the main physical parameters has been shown.

Keywords: Three-dimensional dual boundary elements method · Quasi-Static load · Viscous fluid · Hydraulic fracturing · Non-planar fracture propagation

1 Introduction

In the paper [2] a fully 3D numerical model of fracture propagation from the cavity in an elastic media caused by the viscous fluid pumping was developed

N. Danaev et al. (Eds.): CITech 2015, CCIS 549, pp. 143–157, 2015.
DOI: 10.1007/978-3-319-25058-8_15

and verified. Numerical model means linked submodels and numerical methods and algorithms for their coupled solution. Three basic submodels were linked together into a single model of propagation: the stress-strain state of the elastic media, Newtonian fluid flow, and brittle fracturing and crack growth. The following assumptions were made in the model [2]. The media fracturing velocity is assumed to be low enough. It allows using the fracture propagation the elastic equilibrium equations and the static criteria of crack growth and direction for the fracture propagation simulation. During the model of fracture propagation development authors of [2] were using conventional BEM for the stress-strain state calculations [3]. Therefore this method was used for the elasticity problem solution. However the conventional BEM cannot be used for the line cracks because the integral boundary equation degenerates. Therefore in paper [2] the fracture was considered as a cavity with small but finite width between its sides (Fig. 1). So the fracture was approximated by the crack with the artificial width, and the width itself was defined from the condition of the solution error minimization, caused by this fracture approximation.

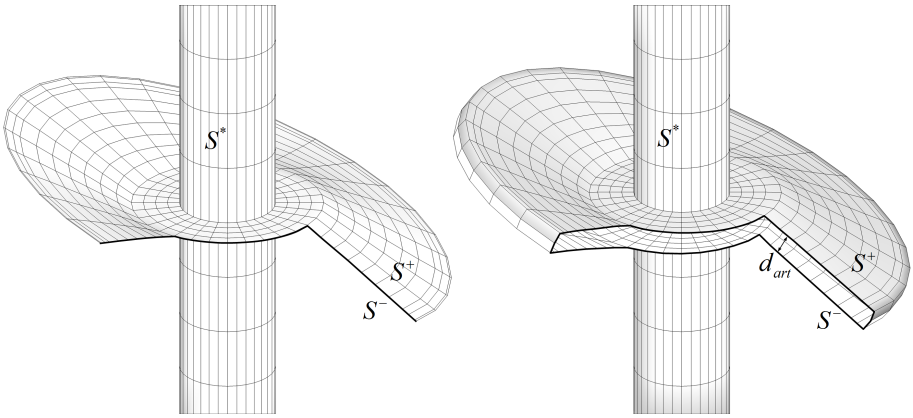

Fig. 1. Artificial notch concept: real fracture (left) is replaced with artificial notch (right) [2].

In the present paper the fracture is treated as a real crack with infinite small distance between sides. For the solution of the elasticity problem with the cavity and the fracture, the modification of the Dual BEM with discontinuous elements is built [4]. It is the most optimal method with regard to the computational costs and the convenience of the integral equations approximation. Near the crack front special elements are used. They account the singularity of the elasticity problem solution. To improve the accuracy of the Stress Intensity Factors calculation, the special boundary elements near the crack front are accounted in the interpolation formulae.

2 Dual BEM

The elasticity problem is solved in an infinite domain with the cavity bounded by S^* and the fracture with sides S^+ and S^- which adjoins the cavity (see Fig. 1, left). Stress-strain state of a media is described by elastic equilibrium equations

$$\frac{\partial \sigma_{ij}}{\partial x_j} = 0, \tag{1}$$

where σ_{ij} are the components of the stress tensor; indices i, j posses the values $1, 2, 3$. The Hookes law for the isotropic homogeneous material is used with the equation (1)

$$\sigma_{ij} = \lambda \delta_{ij} \varepsilon_{kk} + 2\mu \varepsilon_{ij}, \tag{2}$$

where $\varepsilon_{ij} = 0.5(u_{i,j} + u_{j,i})$ are the displacements tensor components, u_i are the components of the displacements vector, δ_{ij} -is the Kronecker symbol, λ and μ are the Lame parameters.

To obtain the closed differential problem let us add the boundary conditions on the cavity surface $S^* = S^t + S^u$

$$t_i\Big|_{S^t} = t_i^*, \quad u_i\Big|_{S^u} = u_i^*, \tag{3}$$

on the fracture sides $S^{\pm}$

$$t_i\Big|_{S^{\pm}} = -p_{crack} n_i, \tag{4}$$

and on the infinite distance

$$u_i\Big|_{S^{\infty}} = 0, \tag{5}$$

to the differential equations (1),(2).

Conventional BEM [5] is used to solve the elasticity problems with a regular boundary S^*. For the problems with fractures $S^{\pm}$ a modification of the conventional BEM – the Dual BEM is suggested in [4]. In DBEM the Displacements Boundary Integral Equation (DBIE) is solved on the regular boundary and the Traction Boundary Integral Equation (TBIE) is solved on the fracture boundary. To solve the elasticity problem near the fracture in an infinite elastic media a modification of DBEM is developed in the present paper.

For points $\mathbf{y}$ at the regular boundary S^* the DBIE is solved

$$\begin{aligned} c_{ij}(\mathbf{y}) u_i(\mathbf{y}) = \int\limits_{S^*} U_{ij}(\mathbf{y}, \mathbf{x}) t_i(\mathbf{x}) dS(\mathbf{x}) - \\ - \oint\limits_{S^*} T_{ij}(\mathbf{y}, \mathbf{x}) u_i(\mathbf{x}) dS(\mathbf{x}) - \int\limits_{S^+} T_{ij}(\mathbf{y}, \mathbf{x}) \Delta u_i(\mathbf{x}) dS(\mathbf{x}). \end{aligned} \tag{6}$$

The singular integrals $\oint$ and $\Yup$ are considered in the meaning of the Cauchy and Hadamard principal value, respectively. In DBEM on one side of the fracture

the TBIE is taken instead of the DBIE.

$$t_j(\mathbf{y}^+) = \int\limits_{S^*} L_{ij}(\mathbf{y}^+, \mathbf{x}) t_i(\mathbf{x}) dS(\mathbf{x}) - \\ - \int\limits_{S^*} M_{ij}(\mathbf{y}^+, \mathbf{x}) u_i(\mathbf{x}) dS(\mathbf{x}) - \Xint= \limits_{S^+} M_{ij}(\mathbf{y}^+, \mathbf{x}) \Delta u_i(\mathbf{x}) dS(\mathbf{x}). \tag{7}$$

Here $L_{ij}(\mathbf{y}^+, \mathbf{x}) = D_{kij}(\mathbf{y}^+, \mathbf{x}) n_k(\mathbf{y}^+)$ and $M_{ij}(\mathbf{y}^+, \mathbf{x}) = S_{kij}(\mathbf{y}^+, \mathbf{x}) n_k(\mathbf{y}^+)$, and functions D_{kij} and S_{kij} are obtained from the kernels U_{ij} and T_{ij} by differentiation with respect to the corresponding coordinates and applying the Hookes law [6]. Equation (7) doesn't contain displacement components u_i on the fracture boundary, but allows to determine the unknown components of the displacement discontinuities Δu_i on the boundary.

2.1 Boundary Discretization and Obtaining the System of Linear Algebraic Equations (SLAE)

Let us demonstrate the numerical method of the TBIE (7) solving in the context of fracture $S = S^+ + S^-$. The whole fracture S is approximated with the boundary elements as it is shown in the Fig. 2

$$S \simeq \sum_{e=1}^{N_e} S^e. \tag{8}$$

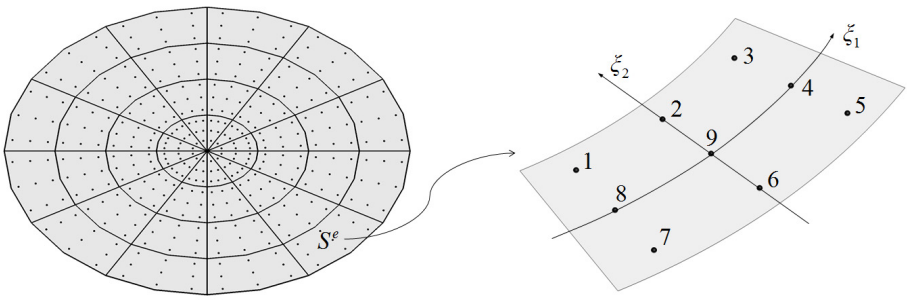

Fig. 2. Segmentation of boundary S into the discontinuous squared boundary S^e (left) and (ξ_1, ξ_2) parameterization of an element with $N_\alpha = 9$ (right).

Each boundary element S^e is parameterized with the local coordinates (ξ_1, ξ_2) as it is shown in Fig. 2. Components of the radius-vectors, displacements discontinuities, and stresses in a certain point of an element (ξ_1, ξ_2) are represented as

$$f_i(\xi_1, \xi_2) = \sum_{\alpha=1}^{N_\alpha} f_i(\mathbf{x}^\alpha) \phi_\alpha(\xi_1, \xi_2), \tag{9}$$

where $\mathbf{x}^{\alpha}$ are the element nodes, $\phi_{\alpha}(\xi_1, \xi_2)$ are the element shape functions, N_{α} is the number of nodes and shape functions in the element.

Equation (7) with respect to the (8) and (9) can be written as

$$t_j(\mathbf{y}^-) = \sum_{e=1}^{N_e} \sum_{\alpha=1}^{N_\alpha(e)} \left(-\Delta u_i^{e\alpha} \int\limits_{\xi_1} \int\limits_{\xi_2} M_{ij}(\mathbf{y}^-, \xi_1, \xi_2) \phi_{\alpha}(\xi_1, \xi_2) J(\xi_1, \xi_2) d\xi_1 d\xi_2 \right), \tag{10}$$

where $J(\xi_1, \xi_2)$ is the Jacobian of the transition to the elements local coordinate system. The displacements discontinuities $\Delta u_i^{e\alpha}$ in the node α of the element e are taken outside the integral because they doesnt depend on the integration variables ξ_1 and ξ_2. Note that integrals in formula (10) depend only on boundary geometry and not on the boundary conditions.

By writing out the equations (10) in the nodes $\mathbf{y}^{e\alpha}$, SLAE for the unknown functions Δu_i is obtained

$$\mathbf{M}\Delta\mathbf{u} = -\mathbf{t}. \tag{11}$$

Here the $\Delta\mathbf{u}$ and $\mathbf{t}$ are the vectors of the displacement discontinuities and tensions in all of the nodes. $\mathbf{M}$ is the matrix, composed of the integral values in equation (10).

In case with cavity and fracture $S = S^* + S^+ + S^-$ the system (11) is written as

$$\begin{bmatrix} \mathbf{T}_{11} - \frac{1}{2}\mathbf{I} & \mathbf{T}_{12} \\ \mathbf{M}_{21} & \mathbf{M}_{22} \end{bmatrix} \begin{pmatrix} \mathbf{u} \\ \Delta\mathbf{u} \end{pmatrix} = \begin{bmatrix} \mathbf{U}_{11} & 0 \\ \mathbf{L}_{21} & -\mathbf{I} \end{bmatrix} \begin{pmatrix} \mathbf{t} \\ \mathbf{t} \end{pmatrix}, \tag{12}$$

where $\mathbf{U}$ and $\mathbf{T}$ are the sub-matrices, composed of the integral values in the DBIE (6), $\mathbf{L}$ and $\mathbf{M}$ are the sub-matrices of the TBIE (7).

2.2 Boundary Elements and Approximating Functions

As long as TBIE (7) requires the smoothness of the surface in the collocation points $\mathbf{y}$ on the fracture $S^{\pm}$, and the elements edges are the lines of discontinuity, DBEM requires to use discontinuous elements with all nodes situated inside the element as it is shown in Fig. 2. In the present paper the discontinuous linear and squared elements, and special elements for the fracture front were used [7]. These elements approximate the displacement discontinuity $\Delta\mathbf{u}$ asymptotic at the fracture front, which improves the accuracy of the Stress Intensity Factors calculations.

2.3 Hadamar Principal Value Calculation of the Singular Integral

The main difficulty of DBEM is to construct the algorithm for the calculation of the Hadamar principal value for the singular integral along the boundary element S^e that appear in the equation (8). The integral contains the collocation point $\mathbf{y}$

$$I_{ij}(\mathbf{y}) = \Xint= \limits_{S^e} K_{ij}(\mathbf{y}, \mathbf{x}) dS(\mathbf{x}). \tag{13}$$

To calculate the integral I_{ij} (13) the singularity substraction technique [8] is used.

3 Calculation of the Stress Intensity Factors

The fundamental postulate of Linear Elastic Fracture Mechanics (LEFM) is that the behaviour of cracks is determined solely by the value of the Stress Intensity Factors (SIFs). The stress field in the vicinity of the crack tip is characterized by the SIFs K_I, K_{II} and K_{III}. In the present paper the displacement extrapolation method for evaluating SIFs is employed [6]

$$K_I^O = \frac{E}{4(1-\nu^2)}\sqrt{\frac{\pi}{2l}}\Delta u_b^P, \tag{14}$$

$$K_{II}^O = \frac{E}{4(1-\nu^2)}\sqrt{\frac{\pi}{2l}}\Delta u_n^P, \tag{15}$$

$$K_{III}^O = \frac{E}{4(1+\nu)}\sqrt{\frac{\pi}{2l}}\Delta u_t^P, \tag{16}$$

where $\Delta\mathbf{u}^P$ is the displacement discontinuity in the fracture point P placed at the distance l from a front point O. Vectors $\mathbf{b}$, $\mathbf{n}$ and $\mathbf{t}$ are local basis on the crack front. Formulae (14), (15), (16) are applicable if the distance l is small enough comparing to the typical fracture size. If the distance l is long, then the SIFs values become understated. In this case the extrapolation of the SIFs values K^{P_1} and K^{P_2}, from the points P_1 and P_2 to the front point O should be used (Fig. 3). Distance to the P_1 and P_2 is l_1 and l_2, respectively.

$$K^O = K^{P_2} + \frac{l_2(K^{P_1} - K^{P_2})}{l_2 - l_1}. \tag{17}$$

To verify the DBEM and the SIFs calculation method the following problem is considered. In the infinite media stretched by tensile stress σ in the direction y the penny-shaped fracture of radius R is placed. The fracture is inclined around the Oz axis at the angle α as it is shown in Fig. 4. The SIFs on the crack front for this problem were previously determined exactly [9]

$$K_I = 2\sigma\cos^2\alpha\sqrt{\frac{R}{\pi}}, \tag{18}$$

$$K_{II} = \frac{4}{2-\nu}\sigma\sin\alpha\cos\alpha\cos\theta\sqrt{\frac{R}{\pi}}, \tag{19}$$

$$K_{III} = \frac{4(1-\nu)}{2-\nu}\sigma\sin\alpha\cos\alpha\sin\theta\sqrt{\frac{R}{\pi}}, \tag{20}$$

where θ is the angular coordinate characterizing the position of the point at the fracture front.

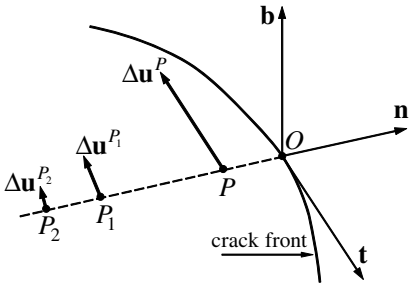

Fig. 3. Method of the displacements extrapolation near the crack front for the SIFs calculation.

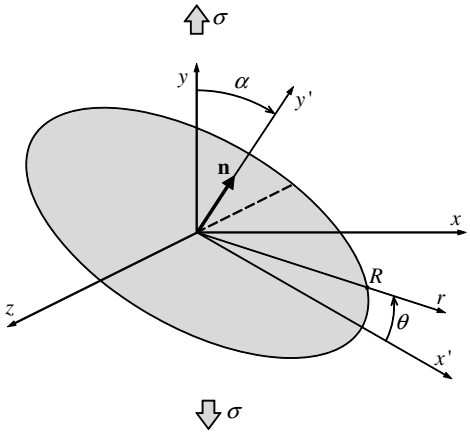

Fig. 4. Problem of a penny-shaped fracture inclined by an angle α under tensile stress σ

Problem is solved numerically on the mesh with 64 elements in the circumferential direction and 16 elements in radial direction. The physical parameters values are $R = 1m$, $p = 1MPa$, $E = 20GPa$, $\nu = 0.2$, $\alpha = 45°$. Figure 5 shows the distribution of the SIFs along the crack front. SIFs are calculated using the special elements and formula (17). Computational error does not exceed 2%.

4 Quasi-Static and Viscous Fluid Fracture Loading

In the case of the high confining stress of deep reservoirs and the low fluid viscosity the fluid pressure along fracture faces is nearly constant. Therefore two models of fracture loading are considered.

In the first one we assume that the fluid pressure is constant along the fracture faces, although it can be time-dependent. Under this condition it is also assumed that fluid and fracture fronts coincide, i.e., the size of so-called fluid lag

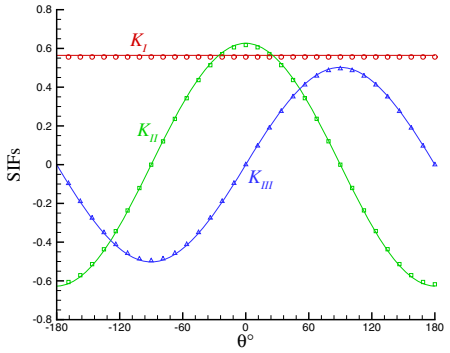

Fig. 5. Dependence of the SIFs from the point position at the front of a penny-shaped fracture: exact solution (solid); K_I (◯), K_{II} (□), K_{III} (△).

is negligible. We consider that hydraulic fracture propagation regime is described by the quasi-static crack growth model.

In the second model the viscous fluid flow inside the fracture is taken into account. In this case the propagation model is unsteady. The process unsteadiness is taken into account by the fluid-flow continuity equation. Meanwhile all other equations describing momentum balance, elastic equilibrium, and material rapture are stationary. The dynamics of the propagation process is represented by the static conditions of flow momentum, stress field, and elastic media displacements in various moments of time.

Fracture surface in 3D space and its piecewise planar representation is shown in Fig. 6. Through the boundary S^q fracturing fluid is pumped from the wellbore to the crack. Boundary S^p is the fluid's front.

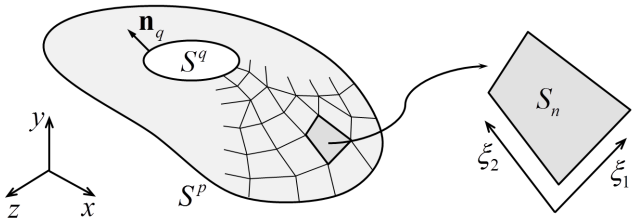

Fig. 6. Fracture surface in 3D space and its piecewise planar representation.

At each planar fracture element the lubrication approximation for a Newtonian fluid flow of viscosity μ between parallel plates, with distance W between each other, gives

$$\mathbf{q} = -\frac{W^3}{12\mu}\nabla p \tag{21}$$

where $\mathbf{q}$ is fluid flux.

The mass conservation equation can be written as follows

$$\frac{\partial W}{\partial t} + \nabla \cdot \mathbf{q} = 0. \tag{22}$$

From (21) - (22) it is possible to obtain the following equation for p:

$$\nabla(a \nabla p) = f, \tag{23}$$

where $a = \frac{W^3}{12\mu}$, $f = \frac{\partial W}{\partial t}$.

Boundary conditions for the equation (23) are the following:

$$p\Big|_{S^p} = p_{pore} \tag{24}$$

and the inflow condition is

$$\int\limits_{S^q} \mathbf{q} \cdot \mathbf{n}_q dS = Q_{in}, \tag{25}$$

Here $\mathbf{n}_q$ is the normal to the boundary S^q. In terms of the pressure the latter condition (25) with consideration of (21) is rewritten as

$$\int\limits_{S^q} a \frac{\partial p}{\partial n} dS = -Q_{in}. \tag{26}$$

It is considered that the fluid front moves with the same speed $\mathbf{v}_f$, as the fluid particles $\mathbf{v}(\mathbf{x})$ at the front do (Stefan condition)

$$\mathbf{v}_f(\mathbf{x}) = \mathbf{v}(\mathbf{x}) = \mathbf{q}(\mathbf{x})/W(\mathbf{x}), \ \mathbf{x} \in S^p. \tag{27}$$

5 Coupling Between Stress-Displacement, Fluid-Flow and Crack Growth Criteria

Let us consider an initial fracture with front defined by the points $\mathbf{x}_i^0$, $i = 1, ..., N_{fr}$. Step-by-step fracture propagation is denoted by superscript n. Fluid front with nodes $\mathbf{x}_{f\ i}^n$, fracture front $\mathbf{x}_{r\ i}^n$, and the lag $L_{r\ i}$ between the fluid and the fracture fronts are introduced into the propagation algorithm. Also the volume V^n of the fluid in the fracture is interacting in the algorithm. It is calculated using the fracture width as

$$V^n = \int\limits_{S^+} W^n dS. \tag{28}$$

The general scheme of the propagation algorithm is shown in Fig. 7. The hydrodynamics-elasticity problem in the algorithm gives the distribution of the

fracture width $W^{n+1\ s}$ and the pressure $p^{n+1\ s}$. Pressure is caused by the fluid flow in the fracture at the fracture front position $\mathbf{x}_{r\ i}^{n+1\ s}$ and the fluid front position $\mathbf{x}_{f\ i}^{n}$. The scheme of the hydrodynamics-elasticity problem solution is shown in Fig. 8. Iteration process $\Delta t^{k+1} = \mathbb{T}(\Delta t^k)$ is introduced to fulfill the condition

$$\max_i \left|\mathbf{v}_i^{m+1\ k}\right| = v_f, \tag{29}$$

which equalizes the maximal fluid velocity at the front and the kinematic condition of the given maximal front increment L_f^0 over the time period Δt that is calculated from the fracture volume dynamics.

With the iterations

$$L_i^{s+1} = \mathbb{L}(L_i^s), \quad \theta_i^{s+1} = \mathbb{Q}(\theta_i^s) \tag{30}$$

the following conditions are fulfilled in the algorithm Fig. 7

$$K_I(\mathbf{x}_i^{n+1\ s}, p^m) = K_{Ic}, \quad K_{II}(\mathbf{x}_i^{n+1\ s}, p^m) = 0 \tag{31}$$

in each of the fracture front nodes on the $n+1$-th propagation step. Iteration schemes (30) are based on the solution methods for the equations (31) correspondingly.

6 Results of Fracture Propagation Simulating

Figures 9 – 11 show the simulation results of the quasi-static propagation of the penny-shaped fracture with radius R from the wellbore with radius R_w. The initial fracture is perpendicular to the axis of the wellbore, which is inclined at the angle α to the vertical direction (axis Oy). Parameter values during the simulation are $E = 20GPa$, $\nu = 0.2$, $K_{Ic} = 3MPa\sqrt{m}$, $R = 1m$, $R_w = 0.5m$, $\alpha = 30°$.

The isometric projections of the fracture during the quasi-static propagation are shown in Fig. 11. The fracture is propagating with constant in situ stress $\sigma_x^\infty = \sigma_z^\infty = 16MPa$, and various in situ stress $\sigma_y^\infty = 8MPa$ (left) and $15.9MPa$ (right). The trajectories in the plane $z = 0$ are also compared in the figure.

The comparison of the quasi-static and the fluid-flow approach to the simulation of the fracture propagation is shown in Fig. 12. Wellbore is inclined against the σ_y^∞ direction at the angle $\alpha = 45°$ as it is shown in Fig. 9. Fluid with viscosity μ is pumped into the wellbore with rate $Q_{in} = 1 \cdot 10^{-3} m^3/s$. Rock is compressed by vertical $\sigma_y^\infty = 12MPa$ and two horizontal $\sigma_x^\infty = 16MPa$ and $\sigma_z^\infty = 16MPa$ stresses. The wellbore height and radius are $H = 5m$, $R_w = 0.5m$. The incipient fracture radius is $R = 1m$. The dynamic fluid flow approach is applied with the two values of fluid viscosity $\mu = 100$ and $1000Pa \cdot s$.

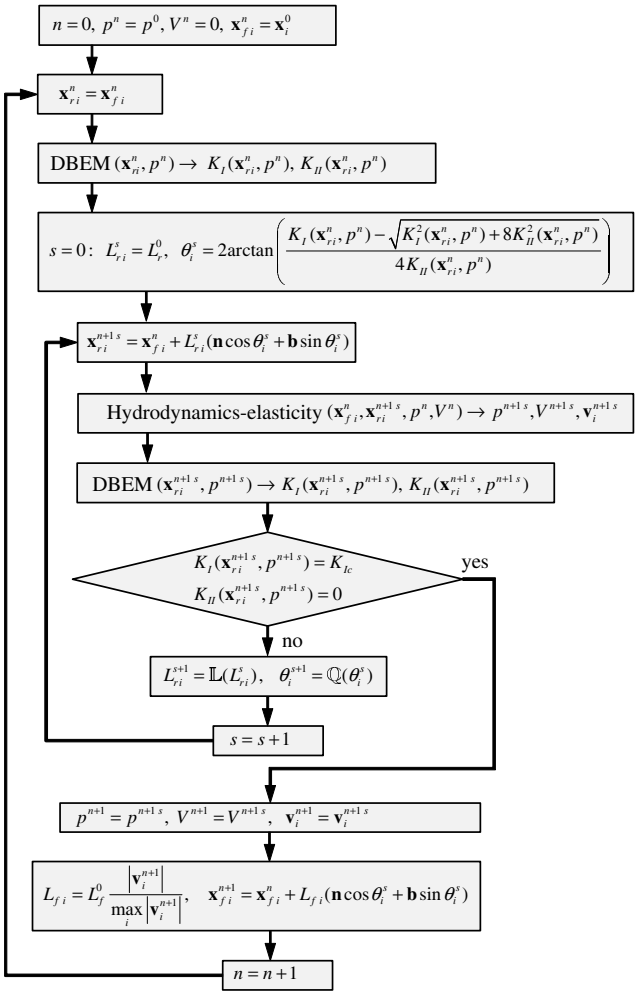

Fig. 7. The fracture propagation algorithm flow chart.

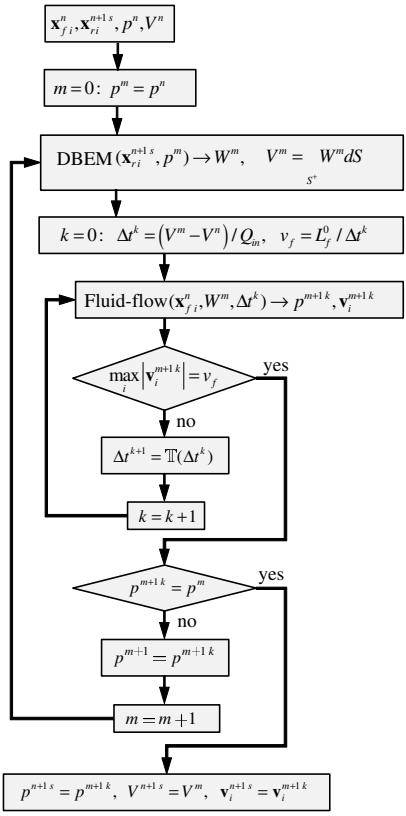

Fig. 8. The flowchart for the hydrodynamics-elasticity problem solution.

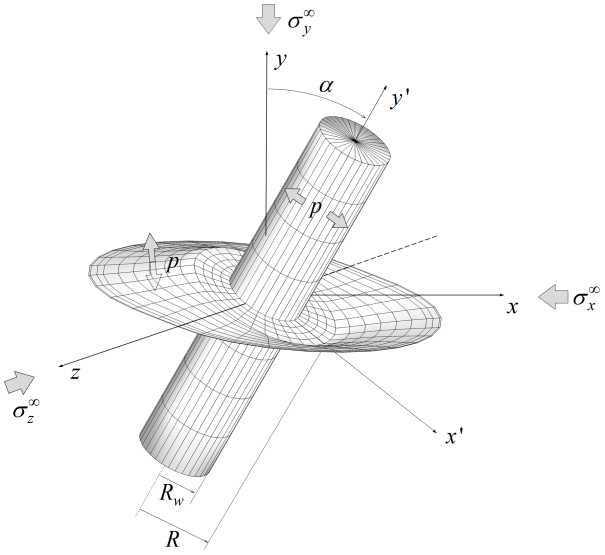

Fig. 9. Cavity and fracture loaded with pressure p in a media, which is compressed by a tensor $\boldsymbol{\sigma}^\infty$ on an infinite distance: $\sigma_x^\infty = -16MPa$, $\sigma_y^\infty = -12MPa$; $\sigma_z^\infty = -16MPa$

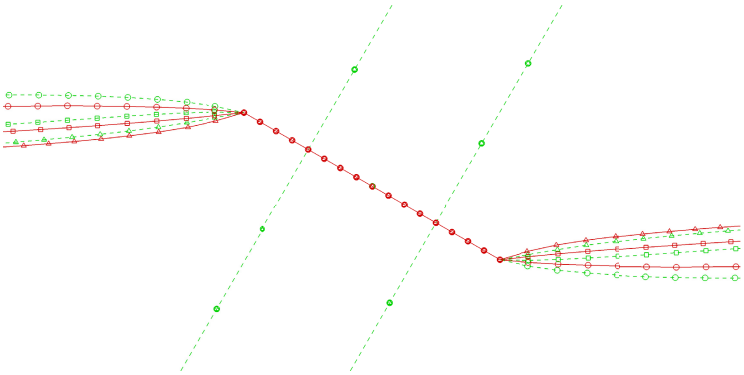

Fig. 10. Fracture trajectories in problems with the wellbore (dashed line) and without (solid line): $(\sigma_x^\infty; \sigma_y^\infty; \sigma_z^\infty) = -(4;3;4)MPa$ (◯), $-(8;6;8)MPa$ (□), $-(16;12;16)MPa$ (△).

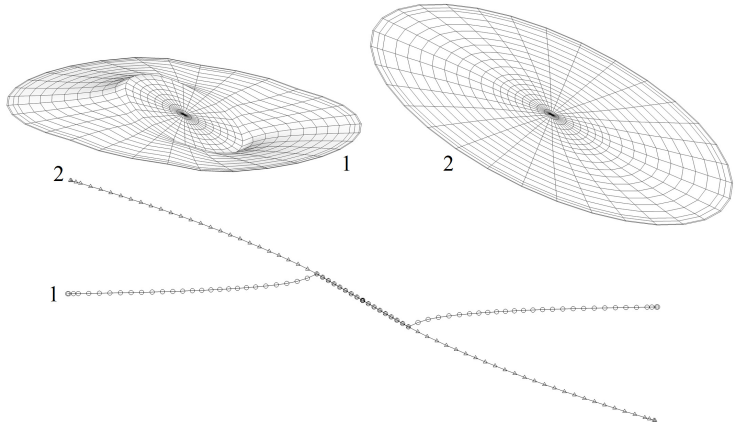

Fig. 11. The quasi-static fracture propagation: 1 – $\sigma_y^{\infty} = 8MPa$ (left); 2 – $\sigma_y^{\infty} = 15.9MPa$ (right); the trajectories in the section $z = 0$ (bottom).

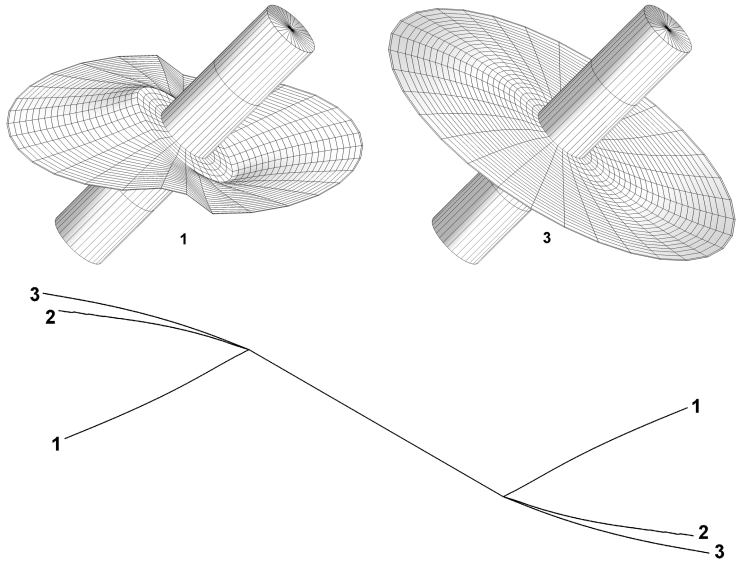

Fig. 12. Fracture trajectories and their cross-sections: 1 - quasistatic approach; 2 - dynamic approach $\mu = 100Pa \cdot s$; 3 - dynamic approach $\mu = 1000Pa \cdot s$

7 Conclusions

1. The concept of the 3D non-planar model of fracture propagation in an elastic media and the numerical algorithm for its implementation are proposed.

2. The concept combines models of the main linked problems that affect one another: stress-strain state, fracture loading, destruction of material, and fracture propagation.
3. The main advantage of the proposed conception is the possibility of using various models in every sub-problem without the necessity to rebuild the whole algorithm, which allows advancing from simple models to complex ones easily.
4. The version of the model that combines the sub-models of the elastic equilibrium, Newtonian fluid flow, and the fracture propagation and direction criterion derived from the linear brittle fracture mechanics is implemented.
5. The verification of the model and the sensitivity analysis of the solution from physical and numerical parameters is performed. It is shown that the results obtained are reliable.
6. The next version of the model will use more precise algorithms of SIFs calculations; the Newtonian fluid will be replaced with the non-Newtonian.

Acknowledgments. Authors gratefully acknowledge the support of this research by the Russian Scientific Fund under grant number 14-11-00234.

References

1. Lapin, V.N., Cherny, S.G., Esipov, D.V., Kuranakov, D.V.: 3D model of fracture initiation and propagation from the cavity in the elastic media loaded by constant pressure. In: Proceedeings of VIII Kazachstan-Russian Conference "Mathematical Modelling in Science and Technical Problems of Oil and Gas Industry", vol. 2, pp. 129–132, Jun 20–21, Kazakhstan, Atyrau (2014) (in Russian)
2. Cherny, S.G., Lapin, V.N., Esipov, D.V., Kuranakov, D.S., Avdyushenko, A.Y.: Simulating fully 3D non-planar evolution of hydraulic fractures. Submitted to the International Journal of Fracture (2015)
3. Alekseenko, O.P., Potapenko, D.I., Cherny, S.G., Esipov, D.V., Kuranakov, D.S., Lapin, V.N.: 3D Modeling of fracture initiation from perforated non-cemented wellbore. SPE J. **18**(3), 589–600 (2013)
4. Mi, Y., Aliabadi, M.H.: Dual boundary element method for three-dimensional fracture mechanics analysis. Engineering Analysis **10**(2), 161–171 (1992)
5. Rizzo, F.J.: An Integral Equation Approach to Boundary Value Problems of Classical Elastostatics // Quart. J. of Applied Mathematics **25**, 83–95 (1967)
6. Aliabadi, M.H.: The Boundary Element Method. Applications in Solids and Structures, vol. 2, 598p. John Wiley and Sons Ltd. (2002)
7. Cisilino, A.P., Aliabadi, M.H.: Three-dimensional BEM analysis for fatigue crack growth in welded components. Int. J. for Pressure Vessel and Piping **70**, 135–144 (1997)
8. Guiggiani, M., Krishnasamy, G., Rudolphi, T.J., Rizzo, F.J.: A general algorithm for numerical solution of hypersingular equations. J. Appl. Mech. **57**, 906–915 (1990)
9. Tada, H., Paris, P., Irwin, G.: The Stress Analysis of Cracks Handbook, 3rd edn. ASME Press, NY (2000)